

## DYNAMIC MODELING AND SOIL MECHANICS FOR PATH PLANNING OF MARS EXPLORATION ROVERS

**Brian Trease**

Caltech / Jet Propulsion Laboratory  
Pasadena, CA, US

**Raymond Arvidson**

Washington University  
St. Louis, MO, US

**Randel Lindemann**

Caltech / JPL  
Pasadena, CA, US

**Keith Bennett**

Washington University  
St. Louis, MO, US

**Feng Zhou**

Washington University  
St. Louis, MO, US

**Karl Iagnemma**

MIT  
Cambridge, MA, US

**Carmine Senatore**

MIT  
Cambridge, MA, US

**Lauren Van Dyke**

Washington University  
St. Louis, MO, US

MSC Software 2011 Users Conference, Americas  
October 4-6, 2011  
Costa Mesa, CA

### ABSTRACT

*To help minimize risk of high sinkage and slippage during drives and to better understand soil properties and rover terramechanics from drive data, a multidisciplinary team was formed under the Mars Exploration Rover (MER) project to develop and utilize dynamic computer-based models for rover drives over realistic terrains. The resulting tool, named ARTEMIS (Adams-based Rover Terramechanics and Mobility Interaction Simulator), consists of the dynamic model, a library of terramechanics subroutines, and the high-resolution digital elevation maps of the Mars surface. A 200-element model of the rovers was developed and validated for drop tests before launch, using MSC-Adams dynamic modeling software. Newly modeled terrain-rover interactions include the rut-formation effect of deformable soils, using the classical Bekker-Wong implementation of compaction resistances and bull-dozing effects.*

*The paper presents the details and implementation of the model with two case studies based on actual MER telemetry data. In its final form, ARTEMIS will be used in a predictive manner to assess terrain navigability and will become part of the overall effort in path planning and navigation for both Martian and lunar rovers.*

### INTRODUCTION

Since 2004, the twin rovers dubbed Spirit and Opportunity have been exploring the surface of opposite sides of Mars. Driven via a robust mobility system, the rovers have been conducting scientific experiments focused on understanding the planet's climate history, surface geology, and potential for past or present life. After surviving 25X its target life, the Spirit rover finally completed operations after succumbing to mobility-related embedding. Opportunity continues to drive on, and will soon face rougher terrains and slopes than encountered before, as it climbs the rim of Endeavor crater.

To a large extent, the mission life and science objectives are determined by the robustness and capability of the mobility system, which consists of a rocker-bogie suspension configuration with six wheel drive capability [1]. In addition the outer four wheels have azimuthal actuators to allow arc turns. The rovers have now both operated in mobility regimes beyond the prediction capabilities of the simple analysis tools currently available to engineers. To this end, we have created a software tool named ARTEMIS, which combines the best of classical terramechanics with state-of-the-art multi-body-dynamics commercial software.

The paper presents the details and implementation of the model and software. A first case study specifically addresses the Spirit Rover embedding situation at the "Troy" site on Mars. A second study focuses on simulating the sol (Mars day) 2211 Opportunity terramechanics experiment in which ripple crossing was performed to test the

dynamics across this terrain. This test supports drive planning to the next science destination at Endeavour crater, for which Opportunity must cross at least 7 km and perhaps a thousand ripples at a top speed of ~5 cm/s.

## RECENT MOBILITY CAMPAIGNS

### Spirit Rover

Both rovers have encountered issues with mobility during their missions, with the most serious event occurring when Spirit became embedded starting on sol 1886 (2009-4-23), as depicted in Fig. 1. Spirit was rendered immobile by a sulfate-rich sandy material located on the west of Home Plate at a site called “Troy” [2]. While traveling south toward Goddard and Von Braun for the winter, Spirit had skirted the edge of a bowl-shaped depression (“Scamander Plains”) and broke through a thin surface crust revealing a high-albedo sandy material. Four of the six rover wheels became nearly-completely buried, percent slip was on the order of 95-98%, and images showed that the body may be high-centered on a rock. This is well beyond the range of intended and studied driving conditions.

Realizing the severity of Spirit’s situation, the team temporarily halted driving on sol 1899 to conduct ground-based testing and devise an extrication plan. The key tactics used in the Spirit extrication attempt included use of a “sand box” testing facility at the Jet Propulsion Laboratory, dynamical modeling of commands and simulated rover responses, and planned extrication sequences based on rover planner experience in driving the two rovers on Mars over the past six years.

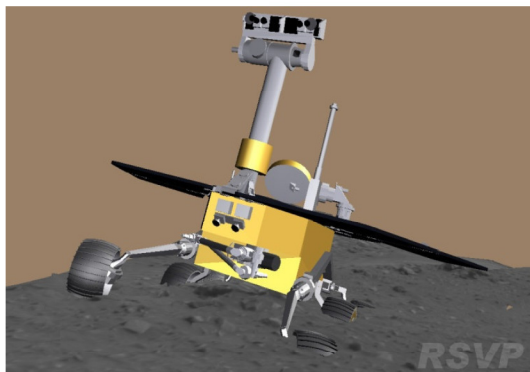


Figure 1: COMPUTER SIMULATION OF SPIRIT’S EMBEDDING

### Opportunity Rover

Opportunity has been traversing the Meridiani plains since January 2004 and after reaching Santa Maria crater on December 16, 2010 had traveled over 26.5 km (based on wheel odometry). With acquisition of stereo imaging before, during, and after drives, together with monitoring wheel turns and currents, suspension angles, and rover attitudes, an extensive data set has been collected to evaluate mobility and to also retrieve terrain and soil properties using basic terramechanics approaches.

Our models have been applied to Opportunity’s drives across the plains since leaving Victoria crater to investigate issues associated with high slippage and sinkage during traverses. Refer to a companion paper at this conference for a more detailed description of the soil and terrain property retrieval [3].

Opportunity’s right front steering actuator failed on sol 433, leaving the wheel rotated inward by ~8 degree angle. The vehicle has primarily been driven backwards during the mission period covered by this paper, in part to minimize wheel actuator current spikes, and because this mode was found to permit Opportunity to cross ripples with minimal mobility difficulties.

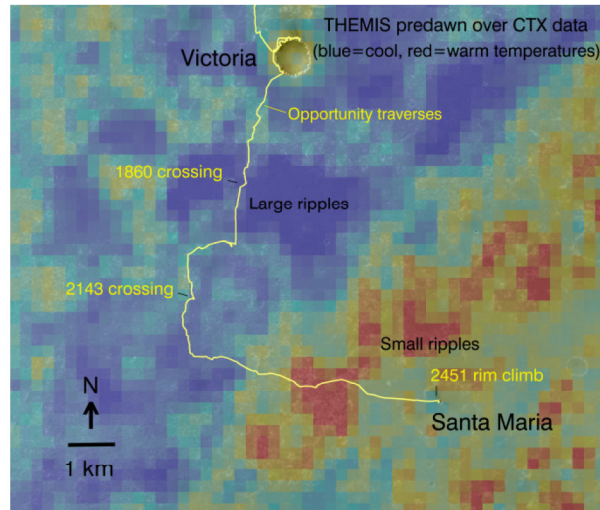


Figure 2: REGIONAL-SCALE VIEW SHOWING OPPORTUNITY'S TRAVERSES BETWEEN VICTORIA TO SANTA MARIA CRATERS. SOLS ARE LABELED FOR WHICH DETAILED DISCUSSION OF HIGH SLIP DRIVES IS INCLUDED IN TEXT. COOL TEMPERATURES IN *THEMIS* PREDAWN *THERMAL INFRARED* CORRESPOND TO LOW INERTIA, LARGE RIPPLES. THIS IS WHERE OPPORTUNITY EXPERIENCED HIGH SLIPPAGE AND SINKAGE.

To reach the Noachian-aged Endeavour crater, traverses needed to be done across rather large aeolian ripple fields (3 to 4 m wide and 10 to 30 cm high) that have relatively low thermal inertias (from *THEMIS*, Mars Odyssey Orbiter's Thermal Emission Imaging System) indicative of loose, poorly sorted sands (Fig. 2) [3]. Largest ripples were avoided and many traverses took place from north to south along inter-ripple corridors. Crossings took place for regions in which relatively low ripples could be found. By sol ~2350, Opportunity arrived at a new terrain type in which ripples were much smaller and thermal inertias higher (Fig. 2).

A detailed analysis of slippage based on visual odometry data collected during drives shows that all the traverses were dominated by relatively low slippage (~5%). High slippage and wheel sinkage values occurred when the rover crossed or straddled large ripples in the area with low thermal inertia. High slippage values also occurred when Opportunity ascended a relatively high slope (~10 deg) to get to the Santa Maria crater rim. In this case the thin soil over bedrock precluded much wheel sinkage. The high slip periods provide information on how the rover's mobility system performs during less than nominal conditions. The modeling tools presented in this paper have provided tactical insight into planning these crossing events with minimal risk to the mission.

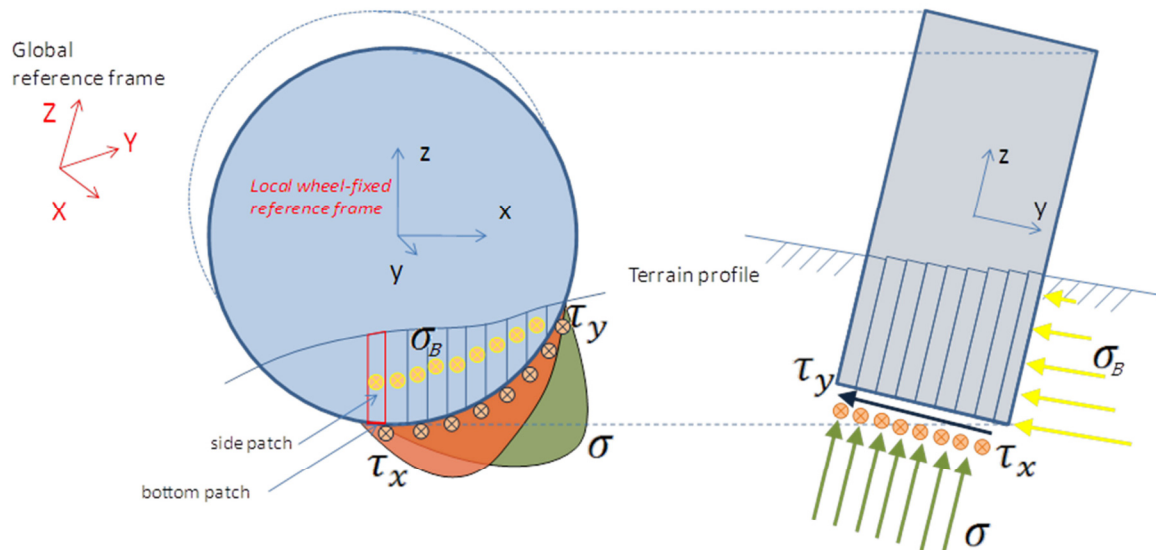


Figure 3: COORDINATE FRAME AND REPRESENTATION OF WHEEL AND SOIL FOR TERRAMECHANICS ANALYSIS

## RELATED RESEARCH

Bekker's original work in the 1950's [5] remains the most cited source for the "classical" semi-empirical equations of terramechanics, later modified by Wong [6-8]. Muro [9] takes an alternate approach to some of these fundamentals, of which we have also incorporated into our modeling tool. Commercial multi-body dynamics software has only recently begun to add soil interaction capability. For example, MSC.Adams provides FTire [10] as an optional add-on, which now includes a basic Bekker-model formulation. Beyond the classical equations, numerous teams are now exploring Discrete Element Modeling (DEM) as a tool for terramechanics simulation. Hopkins and Johnson [11] have simulated a single MER wheel in a soil bed of 400,000 computational particles.

Richter et al. have developed several basic mobility analysis tools that include Bekker's equations and estimations of multi-pass and slip-sinkage events [12]. Further, Krenn and Hirzinger in the German Aerospace Center (DLR) have created their own software that combines a multi-body-dynamics engine, a contact detection algorithm, and an integrated formulation of Bekker's equations, also applied to the simulation of planetary exploration rovers [13].

For additional information, please see Ding et al. [14] for a thorough summary of the above and current research in the field of terramechanics for planetary rovers.

## MODEL OVERVIEW

The foundation of our simulation tool is a 200-element dynamical model of the rover was constructed in Adams software. MSC.Adams is a commercially available software package used for modeling mechanical systems and their interactions with a physical environment. These mechanical models were first presented in 2005 [1,15].

Normal and shear stresses between the wheels and soil were modeled using the classical Bekker-Wong terramechanics expressions that describe relationships among normal and shear stresses, applied wheel torque, wheel slippage and wheel sinkage as a function of soil properties and terrain slope. The complete rover and wheel-soil model was needed, rather than a single wheel model, because of the complex feedback mechanisms between the driven wheels, the suspension system, and the terrain and soils. Lateral and longitudinal stresses, bull-dozing, and skidding were included in the model, all of which are integrated with the Adams model via Fortran subroutines.

## Simplified Contact Model

To provide a baseline and preliminary results, we have implemented two different contact models in our software. The first of these models is the Simplified Contact-based Model, which is included with Adams (Fig. 4). Contact forces between each rover wheel and the soil are defined using a spring model for pressure dependent soil sinkage and Stribeck parameters (static and dynamic coefficients of friction between wheels and soils, together with stiction and friction velocities). In a spring model, when a wheel passes over the soil, the soil compacts in response to the weight of the rover based on the relationship between sinkage and force shown in Fig. 4. However, when that

wheel moves beyond the given area, the soil springs back to its original position. The contact forces between the rover wheels and the soil are simplified, with only one point of contact between each wheel and the soil. Rolling resistance resulting from the wheel penetration is not accounted for.

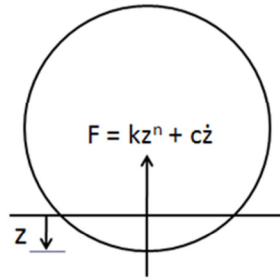


Figure 4: RELATIONSHIP BETWEEN SINKAGE AND FORCE IN THE SPRING MODEL FOR PRESSURE DEPENDENT SINKAGE

### ARTEMIS: Fundamental Equations

Many interpretations of the original Bekker equations are available in the literature; through many iterations of testing our model, we arrived at the selection of a particular subset of formulas described in this section. These include soil-wheel reactions from normal stress, longitude shear stress, lateral shear stress, and bulldozing. These equations allow for the addition of permanent deformation to the pressure dependent sinkage used in the Simplified Contact-based Model. ARTEMIS realistically models compaction sinkage and slip, and it includes the bulldozing effect for longitudinal forces, allowing it to more accurately simulate drives over soft soils.

Figure 3 indicates the chosen coordinate frame and discretization of the wheel and soil. The orientation of the wheel with respect to the local slope is represented as shown in Fig. 5. The free-body diagram for a generalized wheel is shown in Fig. 6.

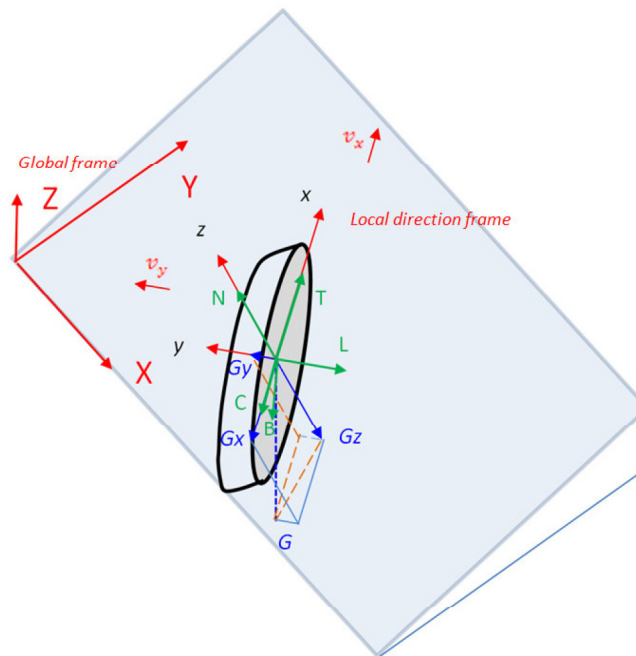


Figure 5: LOCAL (xyz) AND GLOBAL (XYZ) COORDINATES IN ARTEMIS

**Normal Stress.** The normal stress at each bottom contact patch is assumed purely radial, and is calculated using the Bekker-Wong equation [5-7]:

$$\sigma = \begin{cases} \sigma_1 = \left(\frac{k_c}{b} + k_\phi\right) z_1^n & \theta_m < \theta < \theta_f \\ \sigma_2 = \left(\frac{k_c}{b} + k_\phi\right) z_2^n & \theta_r < \theta < \theta_m \end{cases} \quad (1)$$

$$z_1 = r (\cos \theta - \cos \theta_f)$$

$$z_2 = r \left( \cos \left( \theta_f - \frac{\theta - \theta_r}{\theta_m - \theta_r} (\theta_f - \theta_m) \right) - \cos \theta_f \right)$$

where  $\theta_f$  is entry angle,  $\theta_r$  is exit angle,  $\theta_m$  is center angle that maximum normal stress occurs. According to Oida's research,  $\theta_m$  is a polynomial of slip. Ignoring the higher order items results in [5,16]:

$$\theta_m = (a_1 + a_2 l) \theta_f \quad (2)$$

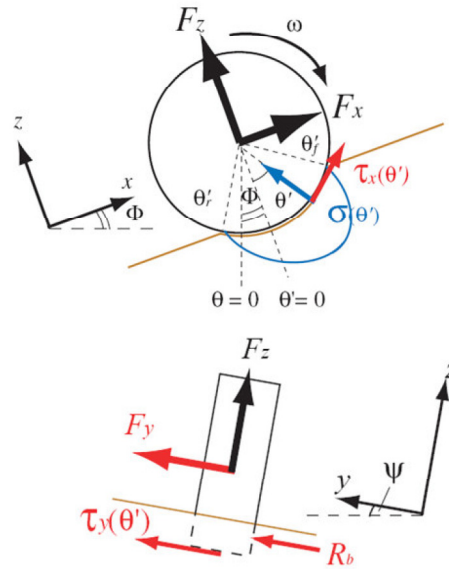


Figure 6 : FREE-BODY DIAGRAM FOR GENERALIZED WHEEL WITH TILT. FIGURES ARE FROM ISHIGAMI [17]

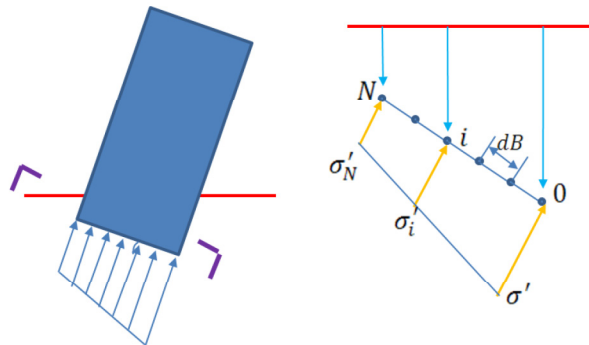


Figure 7: LATERAL WHEEL DISCRETIZATION INTO "SLICES"

The wheel is divided into "slices" normal to the wheel axes (Figure 7) and the entry and exit angle are calculated for each slice. Normal stress in each patch is determined by which slice this patch locates and the center angle for this patch.

**Longitudinal shear stress.** Shear stress in the longitudinal direction (direction of travel) is the primary source of driving traction [18]. Shear stress is function of soil parameters and the measured shear deformation,  $j$ :

$$\tau_x = (c + \sigma \cdot \tan \phi) \left( 1 - e^{-\frac{jx}{k_x}} \right) \quad (3)$$

$$j_x = \int_0^{t_0} v_t dt = \int_{\theta}^{\theta_f} v_t \frac{d\theta}{\omega} \quad (4)$$

where  $v_t$  is the tangential slip velocity and  $k_x$  is the shear modulus. Integrating  $j_x$  over the wheel-terrain geometry shown in Fig. 6 and considering the slip definition given in Equation 21 yields:

$$\text{Driving: } j_x = r \left( \theta_f - \theta - (1 - i)(\sin \theta_f - \sin \theta) \right) \quad (5)$$

$$\text{Braking: } j_x = r \left( \theta_f - \theta - \frac{(\sin \theta_f - \sin \theta)}{i+1} \right)$$

**Lateral shear stress.** Forces in the axial/lateral direction of each wheel are the result of lateral shear stresses, which are calculated in a similar fashion to the longitudinal shear stresses [18-19].

$$\tau_y = (c + \sigma \cdot \tan \phi) \left( 1 - e^{-\frac{j_y}{k_y}} \right) \quad (6)$$

$$j_y = \int_0^{t_0} v_y dt \quad (7)$$

where  $v_y$  is the lateral velocity of the wheel, depicted in Fig. 8.

$$v_y = v_x \tan \beta \quad (8)$$

Integration of Equation 7 leads to closed-form equations for  $j_y$  for slip (driving) and skid (braking) conditions.

$$\text{Driving: } j_y = r(1 - i)(\theta_f - \theta) \tan \beta \quad (9)$$

$$\text{Braking: } j_y = \frac{r(\theta_f - \theta) \tan \beta}{(1 + i)} \quad (10)$$

Shear calculations are performed on discrete “patches” of the wheel mesh and are then summed to provide a single set of forces at the wheel center, as shown in Figure 9.

Integration of Eqn. 6 along the contact patch profile leads to a lateral force component due to shearing action.

$$F_u = br \int_{\theta_r}^{\theta_f} (c + \sigma(\theta) \tan \theta) \left( 1 - e^{-\frac{j_y}{k_y}} \right) d\theta \quad (11)$$

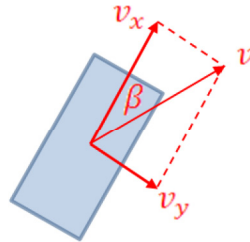


Figure 8: FORWARD AND LATERAL VELOCITY COMPONENTS

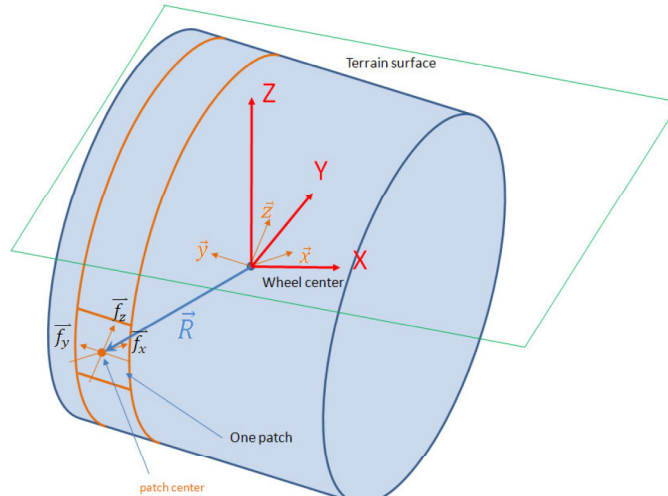


Figure 9: FORCE AND TORQUE CALCULATION AND SUMMATION

**Bulldozing.** Bulldozing forces are computed only in the lateral direction (i.e. on the wheel side walls). These bulldozing forces are modeled as a flat cutting blade moving through soil. The solutions of the cutting blade problem are based on Terzaghi's solution for soil bearing capacity [20]. The basis for calculation is shown in Eqns. 12 and 13, where Terzaghi's equation is presented. This basis is depicted in Figs. 10 and 11.

$$\sigma_B = \gamma z N_\gamma + c N_c + q N_q \quad (12)$$

$$N_\gamma = \frac{2(N_q+1) \tan \phi}{1+0.4 \sin 4\phi} \quad N_c = \frac{N_q-1}{\tan \phi} \quad N_q = \frac{e^{(1.5\pi-\phi) \tan \phi}}{2 \cos^2(\pi/4+\phi/2)} \quad (13)$$

Integrating the predicted stress distribution along the tire sidewall leads to the calculation of lateral force due to bulldozing:

$$F_b = \int_{-r \sin \theta_f}^{r \sin \theta_f} [\gamma N_\gamma f(x) + c N_c + q N_q] f(x) dx \quad (14)$$

where  $f(x) = (\sqrt{r^2 - x^2} - z_0)$ .

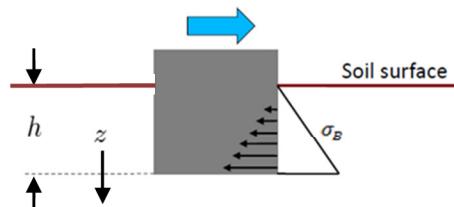


Figure 10: STRESS PROFILE FOR BULLDOZING

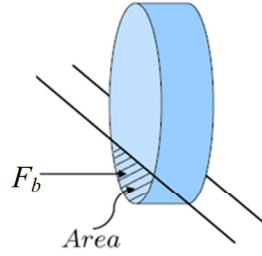


Figure 11: BASIS OF LATERAL BULLDOZING FORCE CALCULATION

**Grouser Effect.** Many planetary rovers include traction features to increase their drive capabilities. The effect of the MER wheel grousers (cleats) on traction was also modeled. The force acting on each grouser ( $F_g$ ) is given by Eqn 15 and depicted in Fig. 12.

$$F_g = b \left[ \frac{1}{2} \gamma h_g^2 N_\phi + 2ch_g \sqrt{N_\phi} \right] \cos \alpha \quad (15)$$

where  $N_\phi = \tan^2(\pi/4 + \phi/2)$ . Grouser influence is modeled after Terzaghi's bearing capacity equation, where  $h_g$  is the height of the grouser and  $\alpha$  is the grouser angle. The force acting on each grouser is decomposed into two directions according to the center angle  $\theta$ . To calculate torque, the net grouser force is applied at a distance equal to  $2/3$  of the grouser's height. (Note that this formulation is exact only when  $\alpha = 0$ ). The total grouser torque is a sum of these individual grouser torques.

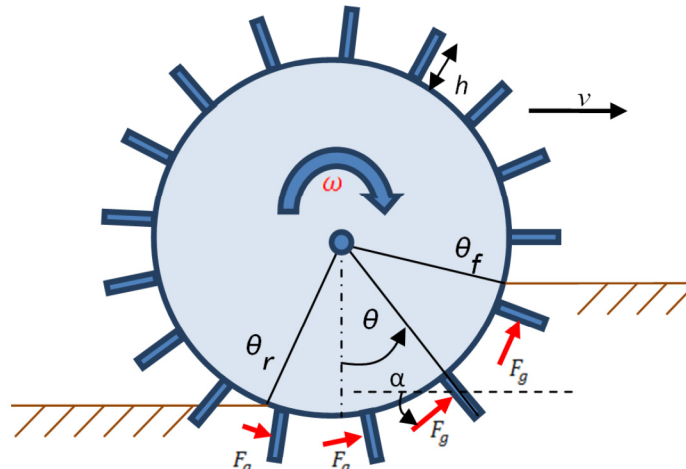


Figure 12: TRACTIVE FORCES DUE TO WHEEL GROUSERS (CLEATS)

**Summations.** The stresses acting over the wheel-terrain contact surfaces are resolved along the normal, longitudinal, and lateral wheel directions, and then summed to compute net forces acting on the wheel.

The thrust,  $T$ , is computed as the sum of all shear force components in the direction of forward wheel motion.

$$T = br \int_{\theta_r}^{\theta_f} \tau \cos \theta d\theta \quad (16)$$

Compaction resistance,  $R_c$ , is the result of all normal force components acting to resist forward motion.

$$R_c = br \int_{\theta_r}^{\theta_f} \sigma \sin \theta d\theta \quad (17)$$

Drawbar pull,  $DP$ , is calculated as the net longitudinal force (i.e. the difference between the thrust force and resistance force).  $DP$  is the resultant force that can either accelerate the wheel or provide a pulling force at the vehicle axle.

$$DP = T - R_c + F_g \quad (18)$$

The lateral force,  $L$ , is computed as the combination of lateral shear forces acting at the wheel-terrain interface,  $F_u$ , and lateral bulldozing forces acting on the wheel sidewall,  $F_b$ .

$$L = F_u + F_b \sin \beta \quad (19)$$

The sum of forces in the normal direction results in the normal force  $W$ , which balances the weight of the rover in the absence of inertial forces.

$$W = br \int_{\theta_r}^{\theta_f} (\sigma \cos \theta + \tau \sin \theta) d\theta + \sum F_g \sin \theta \quad (20)$$

**Slip Modeling.** Of critical importance in the above equations is the proper calculation of slip and skid,  $i$ . The value of  $i$  is bounded from -100% to 100% and represents the effectiveness of the rotary wheel motion in generating forward motion. When angular velocity and forward velocity have the same sign, definitions for slip (driving) and skid (braking) are given in:

$$i = \begin{cases} 1 - \frac{v}{r\omega} & (\text{if } v < r\omega \text{ driving}) \\ \frac{r\omega}{v} - 1 & (\text{if } v > r\omega \text{ braking}) \end{cases} \quad (21)$$

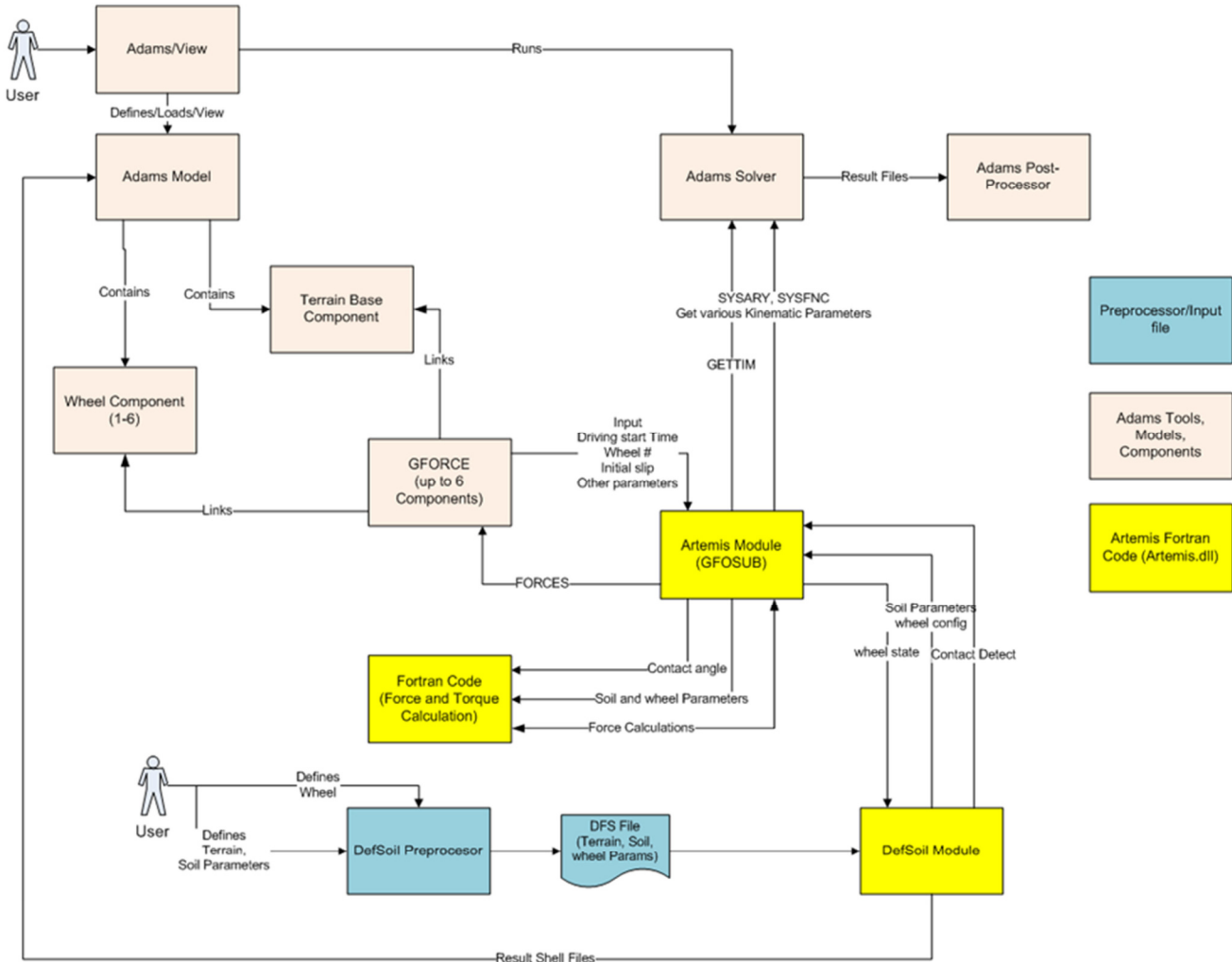


Figure 13 - ARTEMIS ARCHITECTURE

When angular velocity and forward velocity have different signs:

$$i = \begin{cases} 1 + \frac{v}{r\omega} & (\text{if } \frac{r\omega}{v} < -1) \\ -\frac{r\omega}{v} - 1 & (\text{if } -1 < \frac{r\omega}{v} < 0) \end{cases} \quad (21)$$

**Slip Sinkage Effect.** Wheel slip often results in excavation of soil around the wheel, leading to downward wheel displacement termed slip sinkage. ARTEMIS employs a model from [21] for slip sinkage. The amount of slip sinkage is controlled by modifying a soil exponent index, which modulates the soil pressures in Eqn. 1.

$$n = n_0 + n_1|i| \quad (22)$$

## ARTEMIS SOFTWARE DESCRIPTION

ARTEMIS is an extension to the Adams modeling environment designed to model planetary rover-soil interactions. At the core is a dynamic simulation of a rover interacting with a soil. The soil may have multiple soil types and terrain forms. The implementation of ARTEMIS in Adams extends from the previous development and validation of a drop-test model of the MER rovers in Adams.

Figure 13 shows the basic ARTEMIS architecture. At its core, ARTEMIS consists of an Adams model with specific wheel, soil, and force components, a pre-processor program, and a set of Fortran modules assembled into a GFOSUB subroutine that is used by the force component.

Figure 14 shows the basic steps in using ARTEMIS. First, a user will define a soil file (DFS). The DFS file contains the terrain and soil parameters to use in modeling. The ARTEMIS preprocessor is a tool for generating the DFS files. The Wheel Configuration file contains parameters defining the rover wheels. Once both files are created, a user can create an Adams model of the rover or adapt an existing rover model. Simulation and post-processing are both done in Adams.

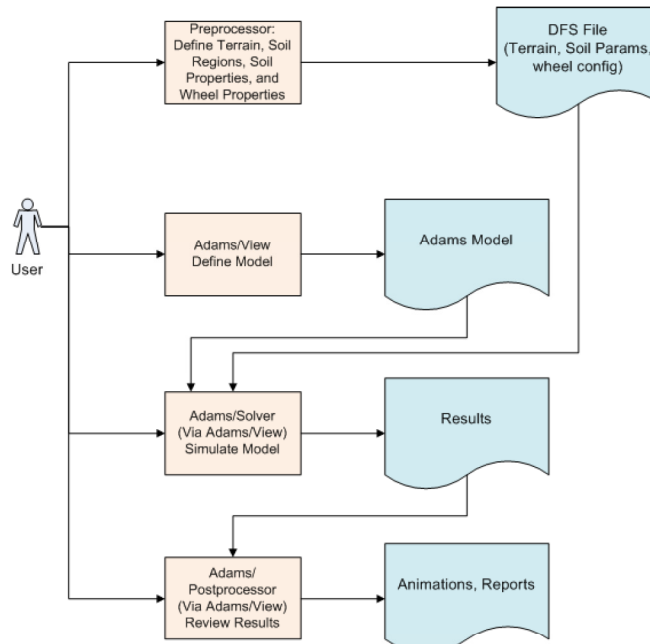


Figure 14: MODELING STEPS

## DEM and Soil Regions

All soils consist of a base Digital Elevation Model (DEM) divided into a set of soil regions. Each soil region has its own set of soil parameters. Base DEMs can be defined using an ENVI geospatial imagery file [22] with a series of soil region masks. All DEMs consist of a set of “cells”, each with a height. Each cell has a width (X) and length (Y) size, and can be defined to have its own unique set of soil parameters.

## ANALYSES AND RESULTS

### Spirit Extraction

Initial simulations have successfully replicated a number of behaviors seen in the JPL sand-box and with Spirit on Mars. These include yaw about the inoperable right-front wheel, translational movement in the downslope direction, excessive (~90%) slip in the drive direction, and a tendency to “pop a wheelie” with the right middle wheel. Low actuator currents associated with recent extrication events for Spirit suggest a similar process has occurred on the right-middle wheel, but without a full wheelie.

A DEM of the terrain directly beneath and around Spirit’s current position was derived from pre-drive Navcam (MER Navigation Camera) images and imported into the model. To increase the fidelity of the model in its current state, wheel tracks (ruts) were manually created by visual inspection of Navcam and Hazcam (MER Hazard Camera) images and are visible in the simulation frames in Figure 15.

The Simplified Contact Model is used in this study. The wheel ruts are modeled using different Coulomb and Stribeck parameters than the surrounding terrain to simulate the lack of crust in those areas. In addition, a first-order approximation of deformable soils within the ruts is achieved by changing the permitted penetration depth and elastic spring constant of the material.

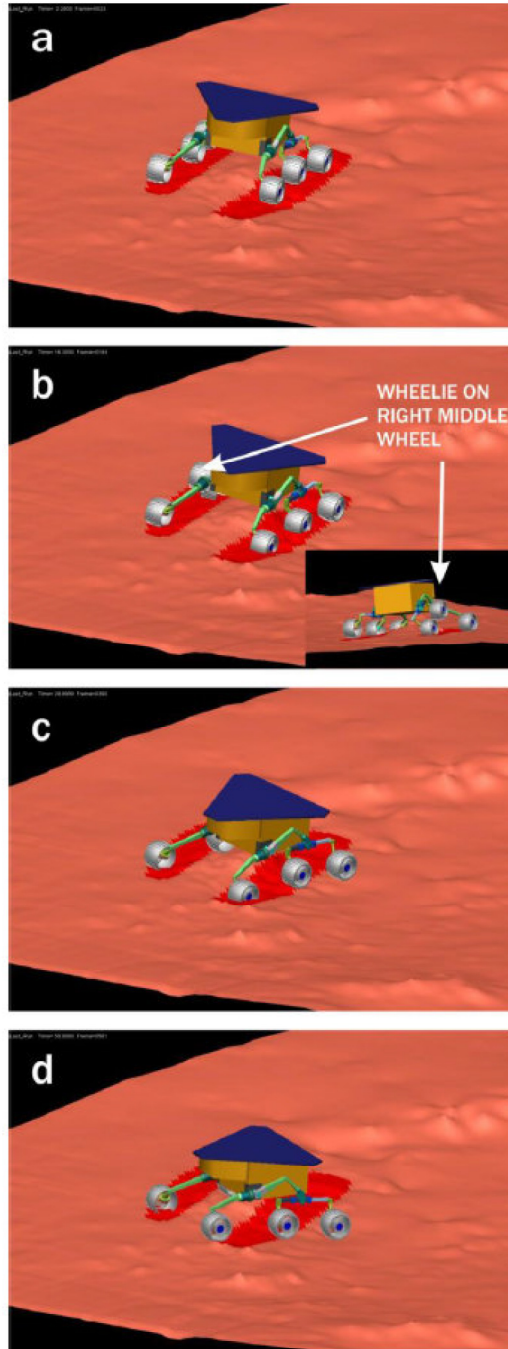


Figure 15: SIMULATION OF SPIRIT ON ITS DRIVE INTO TROY ON SOL 1871 (SIMPLIFIED CONTACT MODEL)

### Spirit four-wheel drives

Additional analyses simulate Spirit four-wheel drives in the sol 1870 DEM in both the Simplified Contact-based Model and in ARTEMIS. These drives were to assess driving strategies for Spirit, should she have become operable again. Spirit's right-front and right-rear wheels (wheels 4 and 6 in the figure) were both inoperable, as reflected in the simulations. A range of friction coefficients for the wheels have been simulated in the contact force model, with the difference between the coefficients for the working wheels and wheels 4 and 6 varied as well. The ranges of friction coefficients tested in these simulations are shown in Table 1.

Table 1: RANGE OF FRICTION COEFFICIENTS TESTED IN SPIRIT FOUR-WHEEL DRIVE SIMULATIONS

Wheel Number	Range for Static Coefficient of Friction	Range for Dynamic Coefficient of Friction
Wheels 4 and 6 (inoperable wheels)	0.6-0.9	0.5-0.8
Healthy Wheels	0.5-0.7	0.4-0.6

Results of these simulations found two common themes in the motion of four-wheel drives: yaw and a stick-slip drive pattern. An example of the yaw resulting from the two inoperable wheels on the rover's right side can be seen in Figure 16 (wheels 4 and 6 are labeled in the first frame).

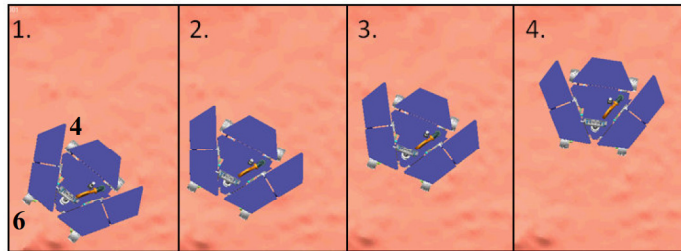


Figure 16: TIME-SERIES IMAGE OF YAW EXHIBITED DURING A FOUR-WHEEL BACKWARD DRIVE SIMULATION.  
 OPERABLE WHEELS: STATIC COF= 0.5, DYNAMIC COF=0.4;  
 WHEELS 4 AND 6: STATIC COF=0.7, DYNAMIC COF=0.6

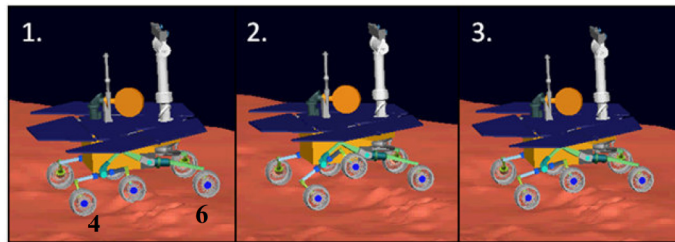


Figure 17: TIME-SERIES IMAGE OF STICK-SLIP MOTION EXHIBITED DURING A FOUR-WHEEL BACKWARD DRIVE SIMULATION.  
 OPERABLE WHEELS: STATIC COF= 0.5, DYNAMIC COF=0.4;  
 WHEELS 4 AND 6: STATIC COF=0.7, DYNAMIC COF=0.6

The drag from wheels 4 and 6 causes the rover to yaw to the left when a straight drive is commanded. (Because this is a simulation of *backward* four-wheel driving, the inoperable right-front and right-rear wheels are seen on the *left* in these images.)

Stick-slip is the other motion that frequently occurred in the four-wheel drive simulations. As resistance builds up on the right-rear wheel (the left front wheel in a backward drive simulation), the middle wheel lifts off the ground and the rover “pops a wheelie,” as shown in Fig. 17 (wheels 4 and 6 are labeled in the first frame). The front wheel then slips forward, lowering the middle wheel until enough force builds up to pop another wheelie.

### Opportunity drive to Endeavor Crater

A second study focuses on simulating the sol 2211 Opportunity terramechanics experiment in which ripple crossing was performed to test the dynamics across this terrain. This test supports drive planning to the next science destination at Endeavour crater. Although a rare occurrence, the rover has encountered high slippage and sinkage problems when climbing the western sides of ripples. The terramechanics modeling provides tactical insight into how to minimize these events.

Figure 18 depicts a time-history of Opportunity crossing a single ripple. A subset of the resulting data attained from the ARTEMIS solver is shown.

### DISCUSSION

Models show that increased wheel sinkage due to increased weight over a given wheel led to increased contact area between the wheel and soil and increased compaction resistance, thereby increasing the amount of slippage for a driven wheel as motor torques are increased to compensate. As slippage increased, additional sinkage occurred as soil was moved in the direction of the spinning wheel. This further increased motion resistance as the wheel came in

contact with additional soil during sinkage. At some point the maximum soil shear stress before failure was reached and slip-page became effectively 100% in some cases, causing longitudinal motion to cease. Models run with real terrain topography derived from stereo image coverage and soil properties dominated by loosely consolidated, poorly sorted sands replicate the main elements of slippage and sinkage (measured from images) and provide validation of the overall modeling approach.

Although they are a good first-order approximation, the built-in Adams contact functions do not address all of the rovers' mobility issues. The ability to model multiple and/or continuous contacts between the wheels and the terrain and to model the terrain as a deformable, changing surface is necessary for accurate and reliable simulation results.

## **FUTURE WORK**

Current ARTEMIS development is centered on assisting Opportunity on its long drive to Endeavor. Work is focused on optimization of ARTEMIS runtime speed and modeling of multi-pass effects. Other topics of interest involve developing parallelized implementations of ARTEMIS, to enable efficient stochastic simulation. Future development will continue to add fidelity to handle deep embedding scenarios such as the Spirit embedding. In its final form, ARTEMIS will be used in a predictive manner to assess terrain navigability and will become part of the overall effort in path planning and navigation for both Martian and lunar rovers.

Detailed simulations are underway to further validate the model and retrieve terrain and soil properties. We expect to be able to simulate traverses of possible ascents of the soil-covered outer rim of Endeavour crater. The ascents will occur after Opportunity leaves Santa Maria and traverses the ~6 km across the plains to get to the Cape York rim segment. Model runs will be used to help define best approaches for ascent, thus minimizing risks to Opportunity's health and safety. Validation of model results is also underway using a simulation of a single rover wheel to compare to laboratory single-wheel testbed data and tests on soil-covered surfaces at JPL using the engineering version of the MER rovers.

## **ACKNOWLEDGMENTS**

While a graduate student at Washington University, Kim Lichtenberg (now at JPL) performed many of the trial runs of early ARTEMIS software. In his role as a rover driver at JPL, Scott Maxwell has continually provided great insight into issues related to rover operation.

A large portion of this research was carried out at the Jet Propulsion Laboratory, California Institute of Technology, under a contract with the National Aeronautics and Space Administration.

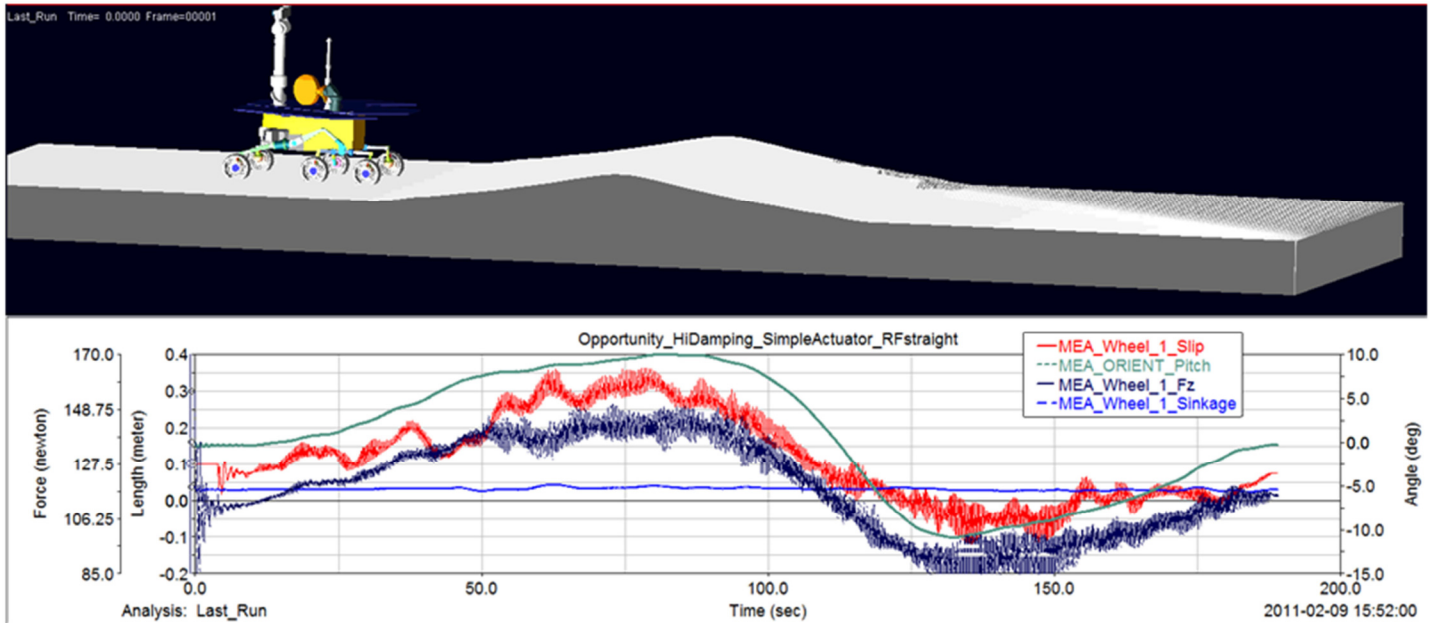


Figure 18: ARTEMIS SIMULATION OF OPPORTUNITY TRaversing A SINGLE RIPPLE. ROVER PITCH AND DATA FOR WHEEL NUMBER 1 ARE PLOTTED AGAINST TIME. WHEEL DATA INCLUDES SLIP, NORMAL FORCE, AND SINKAGE.

## REFERENCES

- [1] Lindemann R. et al., 2006, "Mars Exploration Rover Mobility Development," IEEE Robotics Automation Magazine, 13(2), 19-26.
- [2] Arvidson, R. E., et al. "Spirit Mars Rover mission: Overview and selected results from the northern Home Plate Winter Haven to the side of Scamander crater," *Journal of Geophysical Research—Planets*, Vol. 115, E00F03, doi:10.1029/2010JE003633, 2010.
- [3] Iagnemma, K., Senatore, C., Trease, B., Arvidson, R., Bennett, K., Zhou, F., Van Dyke, L., Lindemann, R., "Terramechanics modeling of mars surface exploration rovers for simulation and parameter estimation," *Proceedings of the ASME Design Engineering Technical Conference*, 2011.
- [4] Arvidson, R., et al., "Opportunity Mars Rover Mission: Overview and Selected Results from Purgatory Ripple to Traverses to Endeavour Crater," *Journal of Geophysical Research—Planets*, Vol. 116, E00F15, doi:10.1029/2010JE003746, 2011.
- [5] Bekker, M.G. *Theory of Land Locomotion*. University of Michigan Press, second edition, 1956.
- [6] Wong, J. Y., *Terramechanics and Off-Road Vehicle Engineering*, 2<sup>nd</sup> Ed., 2010 Elsevier, ISBN 978-0-7506-8561-0
- [7] Wong, J. Y., *Prediction of rigid wheel performance based on the analysis of soil-wheel stresses part I*. Journal of Terramechanics, 1967, Vol. 4, No. 1, pp. 81-98.
- [8] Wong, J. Y., *Prediction of rigid wheel performance based on the analysis of soil-wheel stresses part II*. Journal of Terramechanics, 1967, Vol. 4, No. 2, pp. 7-25.
- [9] O'Brien J. and Muro T.. *Terramechanics: Land Locomotion Mechanics*. Taylor & Francis, 2004, ISBN: 978-9058095725.
- [10] FTire, [http://www.cosin.eu/prod\\_FTire](http://www.cosin.eu/prod_FTire)
- [11] M.A. Hopkins and J.B. Johnson, Discrete Element Modeling of a Rover Wheel in Granular Material Under the Influence of Earth, Mars, and Lunar Gravity, Proceedings of the ASCE Earth & Space Conference, March 2—5, 2008, Long Beach CA.
- [12] Richter L. et al. (2006) 10th European Conference of the ISTVS
- [13] Krenn, R. and Hirzinger, G., "SCM – A soil contact model for multi-body system simulations," *11th European Regional Conference of the International Society for Terrain-Vehicle Systems*, Bremen, October 5-8 2009
- [14] Liang Ding, Zongquan Deng, Haibo Gao, Keiji Nagatani, Kazuya Yoshida, Planetary rovers' wheel-soil interaction mechanics: new challenges and applications for wheeled mobile robots, Intelligent Service Robotics (15 December 2010), pp. 1-22.

- [15] Lindemann R., "Dynamic testing and simulation of the Mars exploration rover," *Proceedings of ASME International Design Engineering Technical Conferences*, pp. 99-106, 2005
- [16] Oida, A., et al, *Three Dimensional Stress Distributions on a Tire-Sand Contact Surface*. Journal of Terramechanics, 1991, Vol. 28, No. 4, pp. 319-330.
- [17] Ishigami, Genya, *Terramechanics-based Analysis and Control for Lunar/Planetary Exploration Robots*, Dissertation, Department of Aerospace Engineering, Tohoku University, March 2008
- [18] Janosi, Z., and Iianamoto, B., "Analytical determination of drawbar pull as a function of slip for tracked vehicles in deformable soils," *Proceedings of the 1st International Conference on Terrain-Vehicle Systems*, Turin, Italy, 1967.
- [19] Ishigami, G., Miwa, A., Nagatani, K., Yoshida, K., "Terramechanics-based model for steering maneuver of planetary exploration rovers on loose soil," *Journal of Field robotics*, Vol. 24, No. 3, 233-250, 2007.
- [20] Terzaghi, K., Peck, R. B., and Mesri, G., *Soil mechanics in Engineering Practice*, John Wiley & Sons, New York, 3<sup>rd</sup> edition, 1996.
- [21] Ding, L., et al, *Wheel slip-sinkage and its prediction model of lunar rover*. Journal of Center South University Technology, 2010, Vol. 17, pp. 129-135.
- [22] ENVI, <http://www.itvis.com/ProductServices/ENVI.aspx>
- [23] R. E. Arvidson, L. van Dyke, K. Bennett, Z. Feng, K. Iagnemma, C. Senatore, R. Lindemann, B. Trease, S. Maxwell, P. Bellutta, A. Stroupe, F. Hartmann, V. Vandi, "Mars Exploration Rover Opportunity terramechanics across ripple covered bedrock in Meridiani Planum," Proceedings of the 40th Lunar and Planetary Science Conference, 2011
- [24] Arvidson, R. E., K. A. Lichtenberg, R. Lindemann, K. Iagnemma, K. J. Bennett, B. Trease, L. Richter, and M. Scharringhausen, 2010b, A Dynamic Model for Assessing Rover Mobility, Abstract submitted to Global Lunar Conference, Beijing, May 2010.
- [25] Shafer, B., et al, *Planetary Rover Mobility Simulation on Soft and Uneven Terrain*, Vehicle Systems Dynamics, Vol 48, No.1, January 2010, pg 149-169